RSC Advances

PAPER

View Article Online
View Journal | View Issue

Check for updates

Cite this: *RSC Adv.*, 2020, **10**, 8332

H_2S detection at low temperatures by Cu_2O/Fe_2O_3 heterostructure ordered array sensors†

Pinhua Zhang,‡[a] Hongyang Zhu,‡[a] Kaifeng Xue,[b] Li Chen,[a] Changmin Shi,[a] Dongchao Wang,[a] Jianfu Li,[a] Xiaoli Wang*[a] and Guangliang Cui*[a]

Received 1st December 2019
Accepted 24th January 2020

DOI: 10.1039/c9ra10054g

rsc.li/rsc-advances

2D heterostructures are promising gas sensor materials due to their surface/interface effects and hybrid properties. In this research, Cu_2O/Fe_2O_3 heterostructure ordered arrays were synthesized using an *in situ* electrodeposition method for H_2S detection at low temperatures. These arrays possess a periodic long range ordered structure with horizontal multi-heterointerfaces, leading to superior gas sensitivity for synergistic effects at the heterointerfaces. The sensor based on the Cu_2O/Fe_2O_3 heterostructure ordered arrays exhibits a dramatic improvement in H_2S detection at low temperatures (even as low as −15 °C). The response is particularly significant at room and human body temperatures since the conductivity of the arrays can change by up to three orders of magnitude in a 10 ppm H_2S atmosphere. These good performances are also attributed to the formation of metallic Cu_2S conducting channels. Our results imply that the Cu_2O/Fe_2O_3 heterostructure ordered arrays are promising candidates for high-performance H_2S gas sensors that function at low temperatures as well as breath analysis systems for disease diagnosis.

1. Introduction

Hydrogen sulfide (H_2S) is a very important environmental and biological marker. Its efficient detection, especially under extreme conditions, has always been an important research area.[1–4] Effective H_2S detection technologies without auxiliary heating supports at low temperatures still deserve to be investigated, and improving the performance of sensitive materials at low temperatures is the prerequisite for achieving breakthroughs in this area.[5,6] Semiconductor gas sensors based on 2D metal oxide nanostructures have been reviewed for the sensitive, selective, and reliable detection of specific gases. One strategy to realize accurate measurements at low temperatures is based on the nanostructure design of 2D metal oxide nanostructures.[7,8] However, progress in the field of functionalized nanostructure design has not conformed to expectations and the structural design of high-performance sensing materials at low temperatures (even below the freezing point) still remains a challenging task.

Because of the linear relationship between the variation in carrier concentration and the magnitude of the adsorption/desorption process, the sensing signal is very limited when the adsorption and desorption processes are fairly weak at low temperatures.[9] Therefore, the introduction of new strategies is imperative to improve the performance and one such strategy is the directed structural design of 2D metal oxide nanostructures.

The heterointerface conductance modulation (HICM) of heterostructure nanoarrays has been proved to be an effective sensing mechanism for low temperature gas detection.[10–12] The heterointerface barrier is sensitive to the carrier concentration; thus, a significant conductance modulation can be obtained even in the case of a small change in the carrier concentration. More importantly, the modulation is almost impervious to temperature. Hence, heterostructure nanoarrays have the ability to convert slight surface absorption signals into strong electric signals under low-temperature conditions. Furthermore, H_2S sensing based on the sulphurization reaction of H_2S and Cu_xO has also been proposed.[11,13,14] The formation of metallic copper sulfide (Cu_xS) conducting channels (CSCC) is bound to cause an obvious change in conductance. Because of the temperature independence and the sulphurization reaction, the sensors based on the Cu_xO nanostructures exhibit superior selectivity and sensitivity at low temperatures.[15,16] However, this detection strategy based on the synergistic effects of the HICM and CSCC mechanisms has not been fully appreciated.

We hope to propose a Cu_2O/Fe_2O_3 heterostructure ordered array, realize the synergistic effect of the HICM and CSCC mechanisms, and achieve H_2S detection at low temperatures (even below the freezing point). The heterostructure ordered arrays are synthesized using the *in situ* electrodeposition method, and the structure and H_2S sensitivity are characterized systematically. The results prove that the Cu_2O/Fe_2O_3

[a]School of Physics and Electrical Engineering, Linyi University, Linyi 276005, China. E-mail: cuiguangliang@lyu.edu.cn; wxl@lyu.edu.cn

[b]School of Mechanical & Vehicle Engineering, Linyi University, Linyi 276005, China

† Electronic supplementary information (ESI) available. See DOI: 10.1039/c9ra10054g

‡ These authors contributed equally to this work.

Open Access Article. Published on 26 February 2020. Downloaded on 12/5/2025 11:06:31 PM. This article is licensed under a Creative Commons Attribution-NonCommercial 3.0 Unported Licence.

This journal is © The Royal Society of Chemistry 2020

Open Access Article. Published on 26 February 2020. Downloaded on 12/5/2025 11:06:31 PM.
This article is licensed under a Creative Commons Attribution-NonCommercial 3.0 Unported Licence.

heterostructure ordered arrays have desirable sensitivity and selectivity towards H_2S at low temperatures (even as low as −15 °C). Meanwhile, the detection performance at room temperature is significantly improved, which presents the potential applications of the Cu_2O/Fe_2O_3 heterostructure ordered arrays in environmental protection and breath analysis systems for disease diagnosis.

2. Methods

2.1. Materials

All chemicals and reagents used in the preparation of Cu_2O/Fe_2O_3 heterostructure ordered arrays were of analytical grade. The chemicals included ferric(III) nitrate nonahydrate ($Fe(NO_3)_3 \cdot 9H_2O$), copper(II) nitrate trihydrate ($Cu(NO_3)_2 \cdot 3H_2O$), and nitric acid (HNO_3). All of the chemicals were purchased from Aladdin. The substrate was monocrystalline silicon with a layer of SiO_2 on the surface, and the electrodes were prepared using Cu foil (99.99%, 30 μm-thick).

2.2. Preparation of Cu_2O/Fe_2O_3 heterostructure ordered arrays

The Cu_2O/Fe_2O_3 heterostructure ordered arrays were synthesized using an *in situ* electrodeposition method in a quasi-2D ultra-thin electrolyte liquid layer. The electrolyte was prepared using $Fe(NO_3)_3$, $Cu(NO_3)_2$, and HNO_3, and the ion concentrations of Fe^{3+} and Cu^{2+} in the electrolyte were 0.04 M and 0.06 M, respectively. The total volume of the electrolyte was 50 mL; 0.1 mL HNO_3 was dropped into 49.9 mL electrolyte to maintain acidity.

At first, the Si substrate was placed on the Peltier element at the bottom of the growth chamber, and two electrodes were placed parallel to each other on the Si substrate. Then, 20 μL electrolyte was dropped onto the Si substrate between the two electrodes. After that, a cover glass was placed onto the two electrodes. A low temperature cycle water bath was used to control the temperature of the growth chamber and freeze the electrolyte, and an ultra-thin ice layer was formed between the silicon substrate and the cover glass. Eventually, two ultra-thin liquid layers of concentrated electrolyte were formed: one between the ice layer and the lower silicon substrate and the other between the ice layer and the higher coverglass. Lastly, the half-sine deposition potential was applied to the electrodes. The electrodeposition process was carried out for about 0.5 h, and the real-time growth process was observed using optical microscopy. When the growth process finished, the coverglass and Si substrate were taken out and cleaned three times with deionized water. Finally, Fe_2O_3/Cu_2O heterostructure ordered arrays were obtained on the surface of the coverglass and Si substrate.

2.3. Characterization

The as-prepared samples were examined by field-emission scanning electron microscopy (SEM, JSM-6700F, JEOL, Japan), transmission electron microscopy (TEM, Tecnai G2, FEI, USA), X-ray photoelectron spectroscopy (XPS, ESCALAB MKII, VG, UK), and scanning probe microscopy (SPM, MicroNano D5A) for morphology, composition, crystallography, and microstructure characterizations.

2.4. H_2S gas response measurements

The samples on the coverglasses were chosen for gas sensing tests. These samples were connected into the circuit by depositing Au film electrodes on both sides of the samples through vacuum ion sputtering. The gas responses were evaluated in a custom-made gas sensing system, which included a test chamber, a Keithley 2400 sourcemeter, and a vacuum cryostat. The gas response is defined as $R = (I_g - I_a)/I_a \times 100\%$, where I_a and I_g are the currents in the air and H_2S atmosphere at a bias voltage of 20 V. The target gases with the desired concentrations were prepared using the static volumetric method. During the H_2S sensing tests, the humidity of the analyte H_2S gases was kept in the range of 50 ± 10%. NH_3 and methanol were used as potentially interfering gases in our tests and were prepared by the evaporation of their solutions in the test chamber. Meanwhile, allochroic silicagel was also placed in the test chamber during the test to keep the humidity constant.

3. Results and discussion

As shown in Fig. 1, samples with different morphologies are deposited using various potentials. The sample was deposited using a semi-sine wave voltage (voltage: 0.3–0.9 V, frequency: 0.6 Hz, as shown in Fig. 1d). The deposition velocity is dependent on the applied potential.[17] When the voltage was small, the ions could migrate to the growth front in time as the deposition process was relatively slow. Therefore, a bamboo-joint-like morphology of the nanoarrays was formed during this deposition process. While the deposition process was relatively fast when the voltage was high, the ions could not migrate to the growth front rapidly enough to keep up with the deposition rate; thus, ridge-like nanowires were formed between the bamboo joints. Furthermore, as we can see in the inset, the nanoarrays have a polycrystalline structure, but the sizes and morphologies of the crystal grains in the bamboo joints and ridge-like nanowires are definitely different.

The deposition potentials of the samples (Fig. 1b and c) were increased from 0.3–1.2 V to 0.3–1.5 V. It can be observed that the cycle length increases gradually as the potential is increased. In addition, it is clearly displayed in the insets of Fig. 1b and c that the crystal grain size of the ridge-like nanowires increases on increasing the deposition potential. Unfortunately, the deposits felled off from the substrate more serious when their size is bigger. Finally, we obtained a uniformly distributed nanowire array with heterointerfaces in the direction of the nanowires. In order to achieve the application of the HICM mechanism in gas sensing, the gas sensors were based on the sample shown in Fig. 1a.

XPS was performed to examine the accurate chemical composition of the Cu_2O/Fe_2O_3 heterostructure ordered arrays. Fig. 2a–c show the high-resolution Cu 2p, Fe 2p and O 1s spectra of the sample. Fig. 2a displays two peaks at 931.6 and 951.4 eV,

Open Access Article. Published on 26 February 2020. Downloaded on 12/5/2025 11:06:31 PM.
This article is licensed under a Creative Commons Attribution-NonCommercial 3.0 Unported Licence.

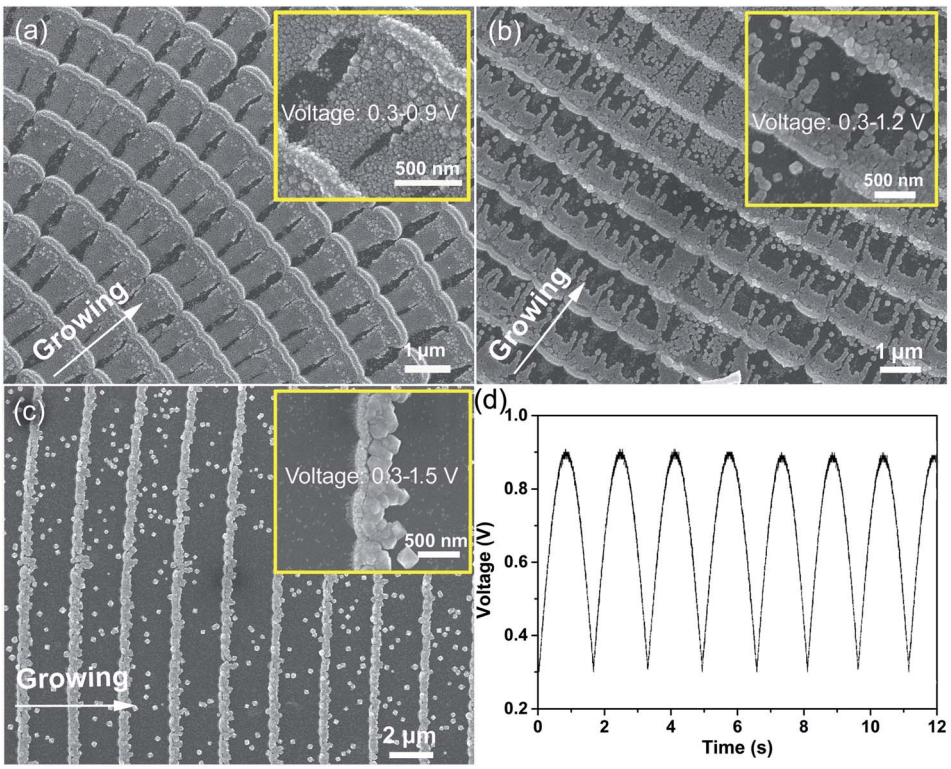

Fig. 1 SEM images of the samples synthesized using different deposition potentials: (a) the voltage was varied from 0.3 to 0.9 V, while the voltage was varied from 0.3 to 1.2 V (b) and 0.3 to 1.5 V (c). The insets in (a), (b), and (c) are the magnification images of each sample. (d) The applied semi-sine wave deposition potential of (a). The period of all potentials was set to a constant value of 0.6 Hz.

corresponding to Cu $2p_{3/2}$ and Cu $2p_{1/2}$, thus proving the existence of Cu_2O.[18,19] As shown in Fig. 2b, the Fe 2p spectrum displays two main peaks at 712.9 and 723.4 eV (corresponding to Fe $2p_{3/2}$ and Fe $2p_{1/2}$) as well as two weak satellite bands associated with these main peaks. This result is in agreement with the values reported in the literature for γ-Fe_2O.[20,21] These binding energies are consistent with those previously reported for Cu_2O and Fe_2O_3, confirming the chemical composition of the Cu_2O/Fe_2O_3 heterostructure ordered arrays. The SAED and HRTEM data shown in Fig. S1† further prove the formation of Cu_2O and Fe_2O_3. In Fig. 2c, the binding energy peak at 529.8 eV is characteristic of the lattice oxygen (denoted as O_L), and the peak at 532.1 eV is assigned to the surface oxygen ions or oxygen vacancies (denoted as O_S).[22] Large numbers of surface oxygen ions and oxygen vacancies on transition metal oxide surfaces play an active role in gas sensing applications.

The structural details of the Cu_2O/Fe_2O_3 heterostructure ordered arrays were confirmed by the energy spectrum analysis of the TEM and SEM data. The TEM image of the sample further reveals the bamboo-like morphology of the heterostructure arrays (Fig. 3a). The element distribution mapping of Cu and Fe in Fig. 3b and c, respectively, shows the differentiated distribution of these two elements. As we can see in Fig. 3b and c, the distributions of Cu and Fe have the same periodicity within the heterostructure arrays. However, the continuity of the distributions is not uniform. The Cu element is continuously distributed in both the bamboo joints and ridge-like nanowires in the sample, while the Fe element is discontinuous in the ridge-like nanowire. More specifically, the distributions of Cu and Fe in the bamboo joints are not synchronized as well; Fe tends to be deposited in the front of the bamboo joint, as shown by the arrows in Fig. 3b and c. The line-profile analysis obtained using energy dispersive spectroscopy (EDS) combined with SEM indicates the same conclusion. As shown in Fig. 3e, the intensity curve of Fe (the blue line) reaches the extremum before that of Cu at the bamboo joint of the sample. The content ratio of Cu_2O to Fe_2O_3 is 4 : 1 according to the EDS and XPS measurements, which confirms that the deposition of Fe_2O_3 is relatively less. This may be one of the reasons for the discontinuous distribution of Fe_2O_3.

Fig. 4 shows the electrostatic field distribution of the Cu_2O/Fe_2O_3 heterostructure ordered array characterized by the electrostatic field microscope (EFM) function of SPM. The 3D stereogram image of the sample and the line-profile analysis path (the red line) are shown in the inset. The heights of the bamboo joint and the ridge-like nanowire are about 130 nm and 50 nm, respectively, and the variation in surface elevation is very regular (black line). Additionally, the data (red line) also reveal that the variation in the electrostatic field has the same oscillation period as the surface elevation and is accompanied by a lag behind the height elevation along the growth direction. In other words, the interface field only exists at the ridge-like nanowires of the arrays due to the discontinuous distribution of Fe_2O_3. Therefore, the Cu_2O/Fe_2O_3 heterostructure ordered

 This journal is © The Royal Society of Chemistry 2020

Open Access Article. Published on 26 February 2020. Downloaded on 12/5/2025 11:06:31 PM.
This article is licensed under a Creative Commons Attribution-NonCommercial 3.0 Unported Licence.

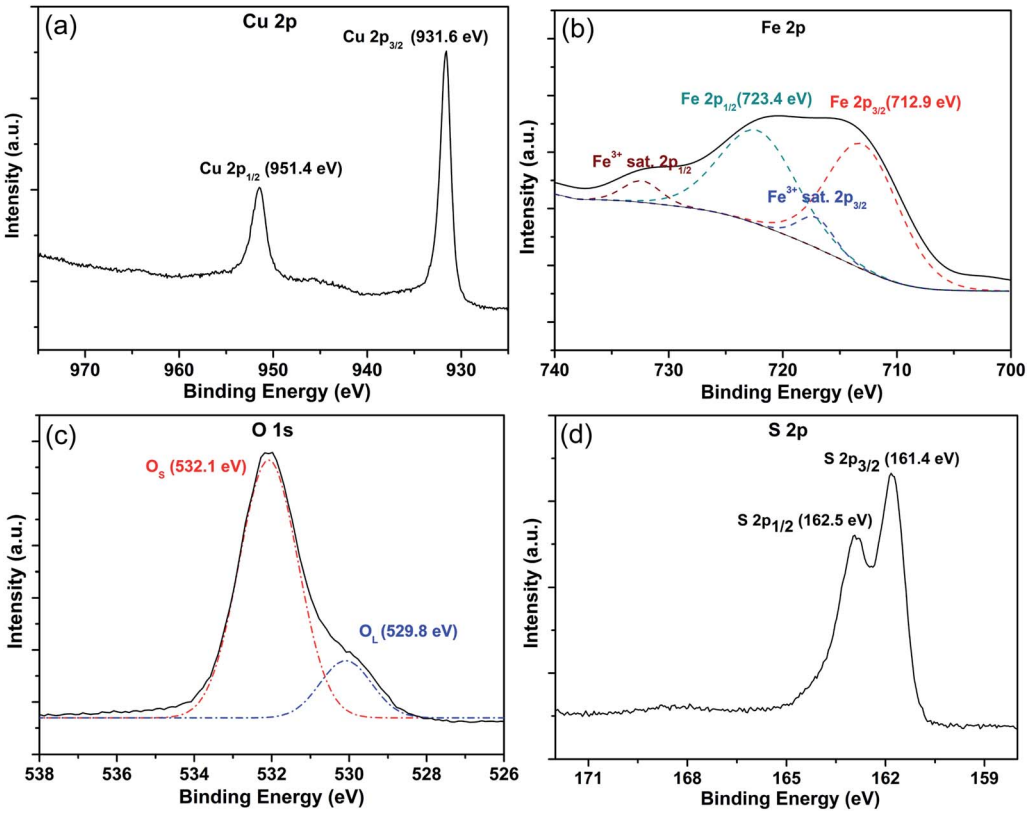

Fig. 2 (a–c) The high-resolution Cu 2p, Fe 2p, and O 1s XPS spectra of Cu_2O/Fe_2O_3 heterostructure ordered arrays before the sensing test. (d) The high-resolution S 2p spectrum of the sample after the sensing test.

arrays can be considered as periodic nano–microstructures based on the alternately distributed Cu_2O (part of the ridge-like nanowire) and Cu_2O–Fe_2O_3 (bamboo joint).

The sensor based on the Cu_2O/Fe_2O_3 heterostructure ordered arrays exhibited excellent H_2S sensing even at low temperatures (Fig. 5). The response of the sensor to 10 ppm H_2S *versus* temperatures between −15 and 65 °C is shown in Fig. 5a. The response increased on increasing the temperature from −15 to 35 °C, while the response marginally decreased at 45 and 65 °C. The data prove the excellent H_2S response of the sensor at low temperatures even at −15 °C ($R \approx 900$). Furthermore, the response reached to the maximum value ($R \approx 14\,200$) at 35 °C; this high response at human body temperature reveals vast potential biomedical applications in the breath analysis of the H_2S biomarker for disease diagnosis. The conductivity of the sensor after being exposed to various concentrations of H_2S at 20 °C is shown in Fig. 5b. The results indicate a good linear response in the range of 20–120 ppm. Above 120 ppm, the conductivity did not change significantly, indicating the saturation of the response. During the H_2S sensing test, the humidity of the H_2S gas was maintained in the range of 50 ± 10%. To evaluate the influence of humidity on H_2S sensing, a series of humidity sensing experiments were conducted on the Cu_2O/Fe_2O_3 heterostructure ordered arrays. As shown in Fig. S2,† the conductance changes slightly as the humidity is varied from 60% to 90% at room temperature. Even when the surface of the sensor was covered with deionized water, the conductance still maintained the same order of magnitude with that at 60% humidity. Thus, the conductance change of the sensor caused by varying humidity can be ignored.

Different gases might lead to changes in the conductance of the Cu_2O/Fe_2O_3 heterostructure ordered arrays due to the sensitivity of Cu_2O and/or Fe_2O_3; thus, the selectivity to H_2S against other potentially interfering gases such as hydrogen (H_2), ammonia (NH_3), methylbenzene (C_7H_8), and methanal (HCHO) was investigated (Fig. 5c).[23–25] It was noted that the as-prepared Cu_2O/Fe_2O_3 heterostructure ordered arrays exhibited a higher response to H_2S at a concentration of 10 ppm at 5 °C compared to that for other tested gases even under more favorable conditions (200 ppm at 10 °C), which confirmed the high H_2S selectivity of the Cu_2O/Fe_2O_3 heterostructure ordered arrays. The curve of conductivity *vs.* response time is shown in Fig. 5d. The conductivity gradually increased when the sensor was exposed to 10 ppm H_2S at −15 °C. The datum exhibits a two-stage response as the frontal curve of the response peak exhibits two distinguished slopes before reaching the plateau region, which indicates the interaction of H_2S and Cu_2O/Fe_2O_3 heterostructure ordered arrays involves two different processes.

We believe that both H_2S absorption and sulphurization of Cu_2O are responsible for the excellent H_2S sensing at low temperatures. In the initial phase of the sensing process, H_2S reacts with the adsorbed oxygen on the surface of the arrays. Therefore, some oxygen-bound electrons can be released back into the surface, which results in a reduction in the holes of p-type Cu_2O. At last, the interface barriers decrease due to the

Open Access Article. Published on 26 February 2020. Downloaded on 12/5/2025 11:06:31 PM.
This article is licensed under a Creative Commons Attribution-NonCommercial 3.0 Unported Licence.

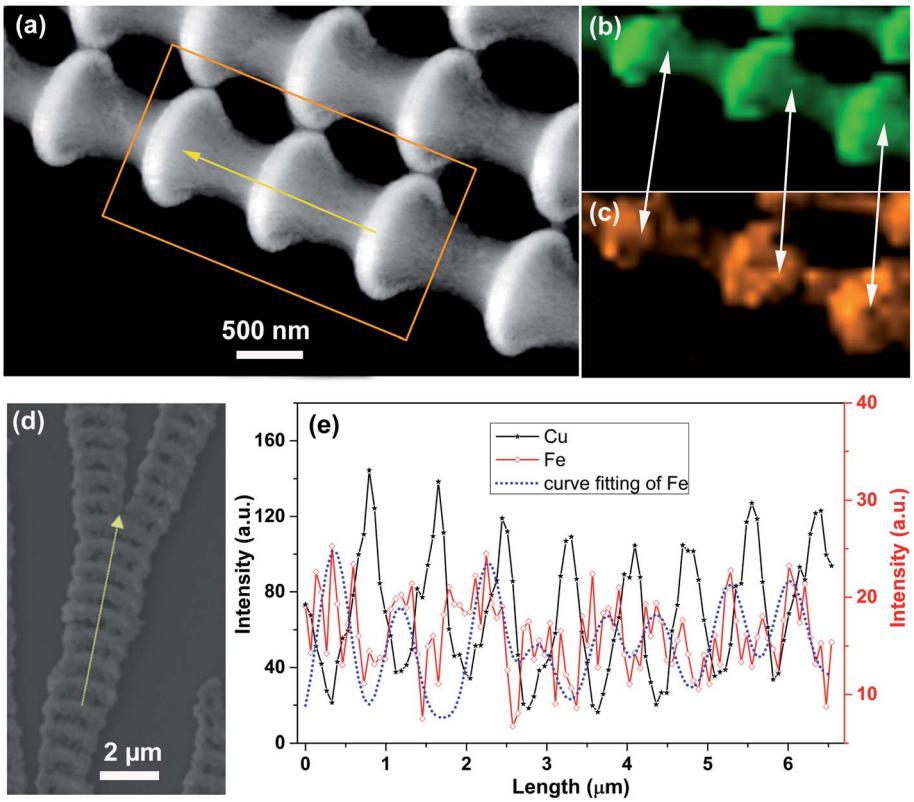

Fig. 3 (a) TEM image of the Cu_2O/Fe_2O_3 heterostructure ordered arrays. (b and c) The distribution of Cu and Fe corresponding to (a). (d and e) Line-profile analysis along the growth direction as well as the distribution of Cu and Fe. The arrows in (a) and (d) indicate the direction of the growth.

reduction in the number of holes, leading to an increase in the conductivity. As we know, such a change in conductivity is not favorable at low temperatures. However, as H_2S absorption increases, H_2S starts to react directly with Cu_2O. This indicates that Cu_2O is converted to metallic Cu_2S through the sulphurization reaction, leading to a remarkable decrease in resistance. Hence, the sensors show a significant response to H_2S.[26,27] The sulphurization reaction of Cu_2O is not sensitive to temperature and perhaps, this is the reason for the excellent H_2S response at low temperatures.

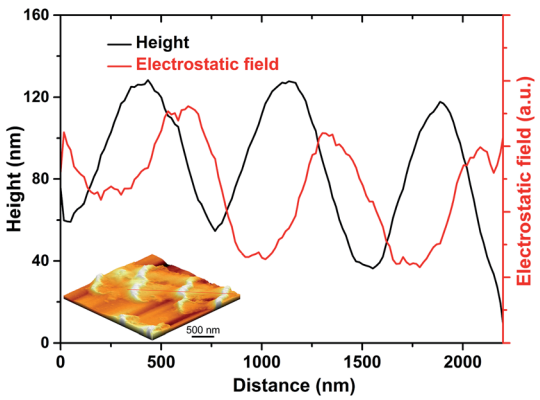

Fig. 4 The distribution of the electrostatic field along with the height variation of the Cu_2O/Fe_2O_3 heterostructure ordered array; the inset is a 3D stereogram of the corresponding test sample.

In order to confirm the sulphurization reaction of Cu_2O, XPS and linear sweep voltammetry (LSV) were further applied to reveal more details of the response. Through the XPS analysis of the samples used for H_2S sensing tests, we can obtain a strong signal of sulphur. As shown in Fig. 2d, the binding energies of the S $2p_{3/2}$ and $2p_{1/2}$ peaks are 161.48 and 162.5 eV, respectively. These binding energies are consistent with those previously reported for S in Cu_2S, indicating the chemical composition of Cu_2S.[18] Moreover, the shape evolution of the *I–V* curves of the sensor supplies further evidence for the presence of Cu_2S. As shown in Fig. 6a, the *I–V* curve of the sensor in air exhibits obvious nonlinear characteristics at −15 °C, indicating the presence of heterointerfaces. This investigation showed that the conductivity of the sensor increased gradually as the H_2S exposure time increased from 120 to 300 s. When the sensor was exposed to 10 ppm H_2S for 120 s (Fig. 6b), the conductivity increased slightly and the *I–V* curve still remained nonlinear. The nonlinear relationship between *I* and *V* began to change when the exposure time increased to 190 s (Fig. 6c), and the conductivity markedly increased. After exposure for 300 s, a standard linear *I–V* relationship was observed (Fig. 6d) with a further increase in conductivity. The transition of the *I–V* relationship indicates a change in the conductive mechanism, which results from the formation of a Cu_2S conducting channel.

 This journal is © The Royal Society of Chemistry 2020

Open Access Article. Published on 26 February 2020. Downloaded on 12/5/2025 11:06:31 PM.
This article is licensed under a Creative Commons Attribution-NonCommercial 3.0 Unported Licence.

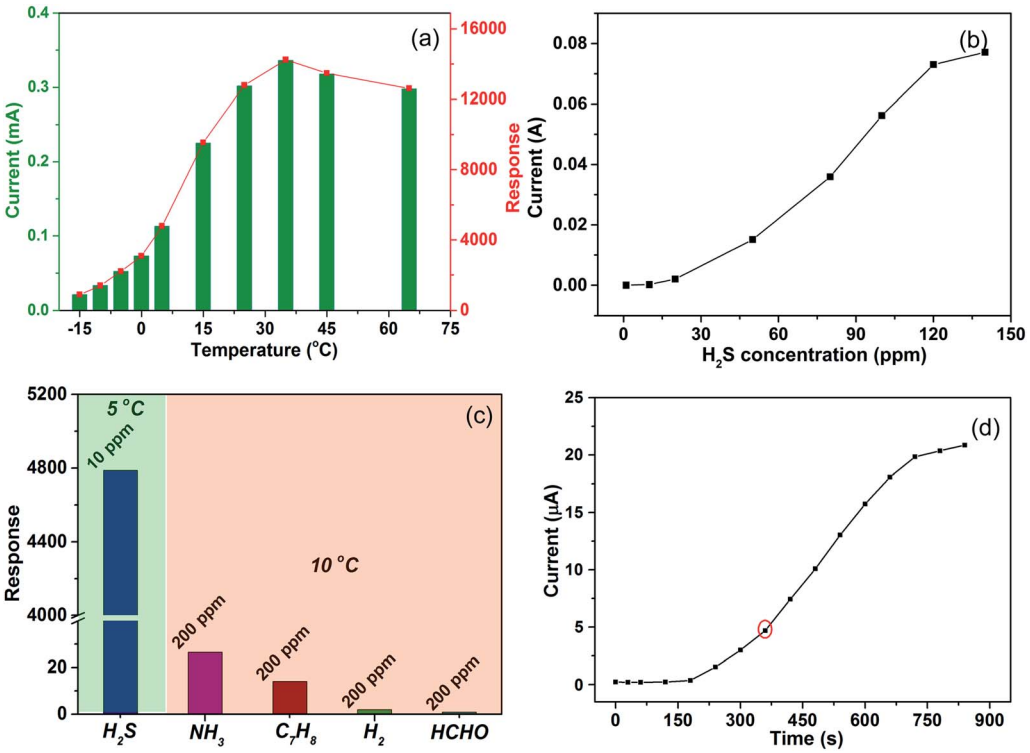

Fig. 5 (a) The temperature dependence of the sensor to 10 ppm H_2S. (b) The sensor response to different concentrations of H_2S at 20 °C. (c) The response of the sensor to 200 ppm NH_3, C_7H_8, H_2, and HCHO at 10 °C and 10 ppm H_2S at 5 °C. (d) Two-stage dynamic response of the sensor to 10 ppm H_2S at −15 °C.

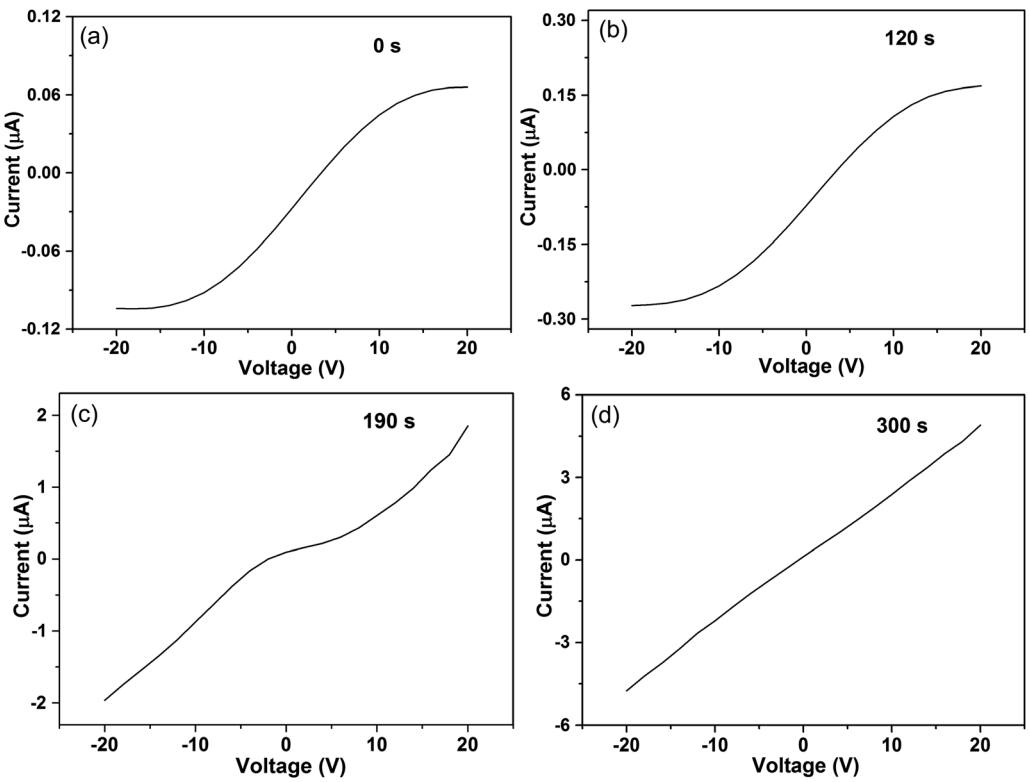

Fig. 6 Linear sweep voltammetry of the sensor in (a) air and 10 ppm H_2S with varying exposure duration times of (b) 120 s, (c) 190 s, and (d) 300 s at −15 °C.

Open Access Article. Published on 26 February 2020. Downloaded on 12/5/2025 11:06:31 PM. This article is licensed under a Creative Commons Attribution-NonCommercial 3.0 Unported Licence.

The details of the two-stage dynamic response of the sensor also prove this point (Fig. 5d). Finally, we can confirm the formation of a continuous Cu_2S conducting channel.

The heterointerface barriers between Cu_2O and Cu_2O–Fe_2O_3 play a key role in the excellent H_2S gas sensing process. These barriers lead to a remarkable increase in the resistance of the Cu_2O/Fe_2O_3 heterostructure ordered arrays. The array is a horizontal heterostructure system, and all heterointerfaces can react with H_2S synchronously. At the initial stage of H_2S absorption, the barriers decreased (but not disappeared), which resulted from the variation in carrier concentration.[28,29] Therefore, the conductivity of the arrays can only change over a small range. With the increase in H_2S absorption, the heterointerface barriers were destroyed due to the formation of the metallic Cu_2S conducting channel. It is worth mentioning that the Cu_2S conducting channel is continuous due to the continuously distributed Cu_2O, leading to a remarkable decrease in resistance. Therefore, the sensor based on Cu_2O/Fe_2O_3 heterostructure ordered arrays shows an enhanced response to H_2S at low temperatures.

4. Conclusions

In conclusion, we have successfully fabricated Cu_2O/Fe_2O_3 heterostructure ordered arrays using the *in situ* electrodeposition method. Based on H_2S absorption/desorption and the sulphurization of Cu_2O, the ordered arrays exhibit excellent H_2S sensitivity at low and human body temperature conditions. The horizontal multi-heterointerfaces and continuous distribution of Cu_2O are the fundamental reasons for excellent performance. These results demonstrate that our fabricated Cu_2O/Fe_2O_3 heterostructure ordered arrays have enormous potential for applications in low temperature H_2S detection and H_2S biomarker testing.

Conflicts of interest

There are no conflicts to declare.

Acknowledgements

This work was supported by the National Natural Science Foundation of China (No. 11704168, 11404158, 11674144, 11634007 and 51431004); Natural Science Foundation of Shandong Province (No. JQ201602, ZR2018MA038, ZR2019MA033 and ZR2016AL09); Shandong Colleges Science and Technology Program (J16LJ04), National College Students' Innovation and Entrepreneurship Training Program (No. 201810452004 and 201810452056).

References

1 M. R. Filipovic, J. Zivanovic, B. Alvarez and R. Banerjee, Chemical Biology of H_2S Signaling through Persulfidation, *Chem. Rev.*, 2018, **118**(3), 1253–1337.

2 T. Xu, N. Scafa, L. P. Xu, S. Zhou, K. A. Al-Ghanem, S. Mahboob, B. Fugetsu and X. Zhang, Electrochemical hydrogen sulfide biosensors, *Analyst*, 2016, **141**(4), 1185–1195.

3 K. Liu, C. Liu, H. Shang, M. Ren and W. Lin, A novel red light emissive two-photon fluorescent probe for hydrogen sulfide (H_2S) in nucleolus region and its application for H_2S detection in zebrafish and live mice, *Sens. Actuators, B*, 2018, **256**, 342–350.

4 Y. Zhang, M. Zhao and D. Chao, A cyclometalated iridium (III) complex for selective luminescent detection of hydrogen sulfide, *Sens. Actuators, B*, 2017, **248**, 19–23.

5 H. Sun, Z. Liu, C. Wu, P. Xu and X. Wang, Amperometric inhibitive biosensor based on horseradish peroxidase-nanoporous gold for sulfide determination, *Sci. Rep.*, 2016, **6**, 30905.

6 Z. Liu, H. Ma, H. Sun, R. Gao, H. Liu, X. Wang, P. Xu and L. Xun, Nanoporous gold-based microbial biosensor for direct determination of sulfide, *Biosens. Bioelectron.*, 2017, **98**, 29–35.

7 J. Chen, L. Xu, W. Li and X. Gou, α-Fe_2O_3 nanotubes in gas sensor and lithium-ion battery applications, *Adv. Mater.*, 2005, **17**(5), 582–586.

8 Y. Zhao, J. G. Song, G. H. Ryu, K. Y. Ko, W. J. Woo, Y. Kim, D. Kim, J. H. Lim, S. Lee, Z. Lee, J. Park and H. Kim, Low-temperature synthesis of 2D MoS_2 on a plastic substrate for a flexible gas sensor, *Nanoscale*, 2018, **10**(19), 9338–9345.

9 G. Cui, P. Zhang, L. Chen, X. Wang, J. Li and D. Wang, Highly sensitive H_2S sensors based on Cu_2O/Co_3O_4 nano/microstructure heteroarrays at and below room temperature, *Sci. Rep.*, 2017, **7**, 43887.

10 H. Huang, H. Gong, C. L. Chow, J. Guo, T. J. White, M. S. Tse and O. K. Tan, Low-Temperature Growth of SnO_2 Nanorod Arrays and Tunable n-p-n Sensing Response of a ZnO/SnO_2 Heterojunction for Exclusive Hydrogen Sensors, *Adv. Funct. Mater.*, 2011, **21**(14), 2680–2686.

11 D. Li, L. Qin, P. Zhao, Y. Zhang, D. Liu, F. Liu, B. Kang, Y. Wang, H. Song, T. Zhang and G. Lu, Preparation and gas-sensing performances of ZnO/CuO rough nanotubular arrays for low-working temperature H_2S detection, *Sens. Actuators, B*, 2018, **254**, 834–841.

12 Q. Zhang, G. Xie, M. Xu, Y. Su, H. Tai, H. Du and Y. Jiang, Visible light-assisted room temperature gas sensing with ZnO-Ag heterostructure nanoparticles, *Sens. Actuators, B*, 2018, **259**, 269–281.

13 N. S. Ramgir, S. K. Ganapathi, M. Kaur, N. Datta, K. P. Muthe, D. K. Aswal, S. K. Gupta and J. V. Yakhmi, Sub-ppm H_2S sensing at room temperature using CuO thin films, *Sens. Actuators, B*, 2010, **151**, 90–96.

14 A. Katoch, S. W. Choi, J. H. Kim, J. H. Lee, J. S. Lee and S. S. Kim, Importance of the nanograin size on the H_2S-sensing properties of ZnO-CuO composite nanofibers, *Sens. Actuators, B*, 2015, **214**, 111–116.

15 Z. Li, J. Wang, N. Wang, S. Yan, W. Liu, Y. Q. Fu and Z. Wang, Hydrothermal synthesis of hierarchically flower-like CuO nanostructures with porous nanosheets for excellent H_2S sensing, *J. Alloys Compd.*, 2017, **725**, 1136–1143.

 This journal is © The Royal Society of Chemistry 2020

Open Access Article. Published on 26 February 2020. Downloaded on 12/5/2025 11:06:31 PM.
This article is licensed under a Creative Commons Attribution-NonCommercial 3.0 Unported Licence.

16 G. J. Sun, S. W. Choi, A. Katoch, P. Wu and S. S. Kim, Bi-functional mechanism of H_2S detection using CuO-SnO_2 nanowires, *J. Mater. Chem. C*, 2013, **1**(35), 5454–5462.

17 Z. Zong, H. Yu, L. Nui, M. Zhang, C. Wang, W. Li, Y. Men, B. Yao and G. Zou, Potential-induced copper periodic micro-/nanostructures by electrodeposition on silicon substrate, *Nanotechnology*, 2008, **19**(31), 315302.

18 V. H. Vinh Quy, J. H. Kim, S. H. Kang, C. J. Choi, J. A. Rajesh and K. S. Ahn, Enhanced electrocatalytic activity of electrodeposited F-doped SnO_2/Cu_2S electrodes for quantum dot-sensitized solar cells, *J. Power Sources*, 2016, **316**, 53–59.

19 H. Zhu, M. Du, D. Yu, Y. Wang, L. Wang, M. Zou, M. Zhang and Y. Fu, A new strategy for the surface-free-energy-distribution induced selective growth and controlled formation of Cu_2O-Au hierarchical heterostructures with a series of morphological evolutions, *J. Mater. Chem. A*, 2013, **1**(3), 919–929.

20 C. Pereira, A. M. Pereira, P. Quaresma, P. B. Tavares, E. Pereira, J. P. Araújo and C. Freire, Superparamagnetic γ-Fe_2O_3@ SiO_2 nanoparticles: a novel support for the immobilization of [$VO(acac)_2$], *Dalton Trans.*, 2010, **39**(11), 2842–2854.

21 D. Ma, T. Veres, L. Clime, F. Normandin, J. Guan, D. Kingston and B. Simard, Superparamagnetic Fe_xO_y@SiO_2 Core-Shell Nanostructures: Controlled Synthesis and Magnetic Characterization, *J. Phys. Chem. C*, 2007, **111**(5), 1999–2007.

22 F. A. C. Pastrian, A. G. M. Silva, A. H. B. Dourado, P. L. Batista, A. G. S. D. Oliveira-filho, D. D. C. Q. Jhon, P. H. C. Camargo, S. Inés and C. D. Torresi, Why Could the Nature of Surface Facets Lead to Differences in the Activity and Stability of Cu_2O-based Electrocatalytic Sensors?, *ACS Catal.*, 2018, **8**(7), 6265–6272.

23 F. Wang, H. Li, Z. Yuan, Y. Sun, F. Chang, H. Deng, L. Xie and H. Li, A highly sensitive gas sensor based on CuO nanoparticles synthetized: via a sol-gel method, *RSC Adv.*, 2016, **6**(83), 79343–79349.

24 X. Gou, G. Wang, J. Yang, J. Park and D. Wexler, Chemical synthesis, characterisation and gas sensing performance of copper oxide nanoribbons, *J. Mater. Chem.*, 2008, **18**(9), 965–969.

25 Y. H. Choi, D. H. Kim, S. H. Hong and K. S. Hong, H_2 and C_2H_5OH sensing characteristics of mesoporous p-type CuO films prepared via a novel precursor-based ink solution route, *Sens. Actuators, B*, 2013, **178**, 395–403.

26 F. Shao, M. W. G. Hoffmann, J. D. Prades, R. Zamani, J. Arbiol, J. R. Morante, E. Varechkina, M. Rumyantseva, A. Gaskov and I. Giebelhaus, Heterostructured p-CuO (nanoparticle)/n-SnO_2 (nanowire) devices for selective H_2S detection, *Sens. Actuators, B*, 2013, **181**, 130–135.

27 S. W. Choi, A. Katoch, J. Zhang and S. S. Kim, Electrospun nanofibers of CuO-SnO_2 nanocomposite as semiconductor gas sensors for H_2S detection, *Sens. Actuators, B*, 2013, **176**, 585–591.

28 H. J. Kim and J. H. Lee, Highly sensitive and selective gas sensors using p-type oxide semiconductors: overview, *Sens. Actuators, B*, 2014, **192**, 607–627.

29 Z. Li, H. Li, Z. Wu, M. Wang, J. Luo, H. Torun, P. Hu, C. Yang, M. Grundmann, X. Liu and Y. Fu, Advances in designs and mechanisms of semiconducting metal oxide nanostructures for high-precision gas sensors operated at room temperature, *Mater. Horiz.*, 2019, **6**(3), 470–506.